Theoretical Study of the Electron Transport in Graphene with Vacancy and Residual Oxygen Defects after High-Temperature Reduction

3 AUTHORS:

Geunsik Lee
Pohang University of Science and Technology
61 PUBLICATIONS **1,159** CITATIONS

SEE PROFILE

Kwang-Sun Kim
Korea University of Technology and Education
555 PUBLICATIONS **30,634** CITATIONS

SEE PROFILE

Kyeongjae Cho
University of Texas at Dallas
302 PUBLICATIONS **9,416** CITATIONS

SEE PROFILE

Theoretical Study of the Electron Transport in Graphene with Vacancy and Residual Oxygen Defects after High-Temperature Reduction

Geunsik Lee,[†,‡] Kwang S. Kim,[‡] and Kyeongjae Cho[*,†]

[†]Department of Materials Science and Engineering and Department of Physics, The University of Texas at Dallas, Richardson, Texas 75080, United States

[‡]Center for Superfunctional Materials, Department of Chemistry, Pohang University of Science and Technology, San 31, Hyojadong, Namgu, Pohang 790-784, Republic of Korea

S *Supporting Information*

ABSTRACT: It is known that a high-temperature reduced-graphene-oxide (HT-RGO) exhibits 3 orders of magnitude increase in the conductivity compared to original graphene oxide but still 3 orders of magnitude below the value of pristine graphene. Substantial amounts of defects that remain in the reduced sample are responsible for the inferior transport quality. On the basis of the defect model which involves C vacancies and the O substitution of edge C atoms, we study the electronic structure and conductivity of HT-RGO using nonequilibrium Green's function theory in tight binding and density functional theory schemes. It is shown that electrons are localized within 10—40 nm due to vacancy defects. We also discuss the transport behavior via such localized carriers in connection with recent experimental findings.
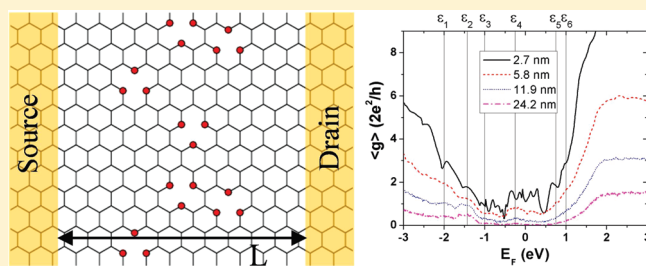
Since the first successful mechanical exfoliation of a single layer of graphene,[1] diverse techniques to acquire large size flakes with good quality at low cost have been reported, such as epitaxial film on SiC,[2] chemical vapor deposition,[3−5] thermal exfoliation,[6] and chemically modified graphene.[7] In particular, the chemical modification of graphite has been significantly advanced for the possible use in device applications. Once a stable aqueous dispersion of oxidized graphite is obtained in the form of an individual graphene oxide sheet, it can be chemically reduced by reducing agents such as hydrazine. A key step lies in preventing the aggregation of the exfoliated graphene sheets after reduction. The reported methods include polymer coating,[8] sulfonation,[9] utilization of $N_2H_4^+$ in hydrazine solvent,[10] and increasing solvent pH.[11] More recently, direct exfoliation of graphite in diverse organic solvents was demonstrated without chemical modification of the graphene sheets.[12]

The electrical property of reduced graphene oxide (RGO) is technologically important. Graphene oxide (GO) shows a conductivity increase by 3 to 4 orders of magnitude after reduction.[13−15] The conductivity of the reduced samples could reach ~1000 S/m which is several % that of graphite.[9,11] This indicates that most of the C−C π bonds are restored after reduction. However, the reported conductivities are quite scattered by about 1 or 2 orders of magnitude variation,[7] and 1000 S/m is still 3 orders lower than the conductivity of mechanically exfoliated sample. Since most samples are prepared in a stack of many small flakes prior to electrical measurement, their electrical conductivity is mostly limited by their percolating nature, i.e., contact resistance between flakes. We also note that a single flake of chemically reduced

graphene has shown a low conductivity of ~100 S/m with the channel-electrode contact effect.[13] The characterizations via Raman, X-ray photoelectron, and infrared spectra revealed that there exists significant disorder and chemical bonds between O and C atoms in the reduced GO samples.[9,10,13,14] The elemental analysis showed that the C/O ratio is about 10:1.[14] This means that the remaining O or structural defects disrupt electron transport in a single flake. Residual O atoms could be eliminated via postannealing at 1100 °C, reaching to less than 1%,[16] where its conductivity was often shown to increase by another factor.

A very recent report demonstrates that as GO is reduced thermally at ~850 °C, it shows a giant infrared absorption by cyclic edge C−O−C etheric groups (where residual O atoms of the 10:1 C/O ratio are present by substituting edge C atoms) at vacancy defects.[17] This intriguing HT-RGO exhibits 3 orders of magnitude increase in the conductivity compared to the original GO, but it is still 3 orders of magnitude below the values reported for the pristine graphene, raising a question about the electron transport mechanism.[13] The atomic structure of the HT-RGO is unknown. Theoretically it is shown that the higher oxidation coverage in the form of epoxide and hydroxyl groups is energetically more favorable.[18] However, in a H_2 environment, such basal plane groups are very likely to form H_2O (3.62 eV energy gain for the reaction: epoxide + H_2 → H_2O, 2.25 eV gain for hydroxyl + $H_2/2$ → H_2O) as we found from the density
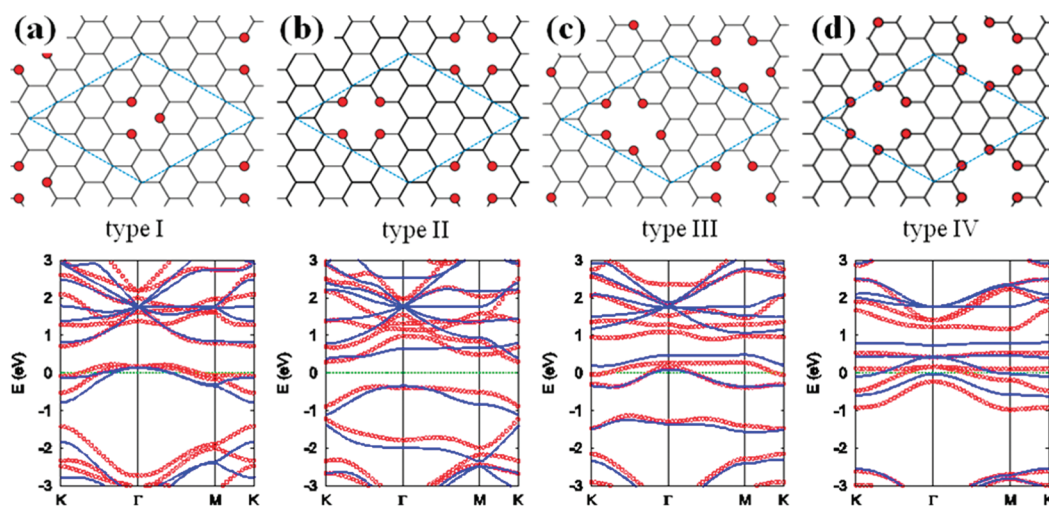
Figure 1. Model structures of reduced graphene oxide with vacancy defects and O substitution of edge C atoms (the red filled circles denote O atoms): (a) single, (b) two, (c) three, and (d) four C vacancies. The 4×4 periodic supercell, indicated by the dashed line, is used to obtain band structures. Their band structures by π-TB (blue solid line) are shown below in comparison with ab initio results (red circles), where original π-TB energy eigenvalues are shifted by -1 eV (see the text).

functional theory (DFT) study on their stability. This result means that most basal plane groups will be reduced, and topological defects (e.g., missing carbon atoms) could be one of the main factors for the reduced electrical conductivity. OH radicals can easily create vacancy defects, which in turn can be very reactive toward further oxidation.[19] The molecular dynamics simulation of the oxidized graphene in the presence of vacancies shows that O atoms strongly tend to bond to C atoms with dangling bonds, causing five- or six-membered rings and carbonyl groups.[20] We note that such edge O groups have 5−7 eV higher binding energies than those of epoxide or hydroxyl on the basal plane. Relatively weakly bonded oxygen groups on the basal plane will be released from graphene sheets easily, as shown experimentally by a sharp mass loss near $T = 200 \,^{\circ}\mathrm{C}$.[21] Meanwhile, the edge oxygen groups remain bonded to carbon rings up to 800 °C, giving 10:1 C/O ratio at the end of the thermal annealing. Especially, the final form of the oxygen group after thermal reduction is the cyclic edge etheric group C−O−C.[17]

The electron transport mechanism in such seemingly highly disordered RGO is one important concern. The major defects to be considered are atomic scale defects, that is, vacancy and residual O substituting C atoms, where such defects are shown to cause both intervalley and intravalley scatterings.[22] According to the theoretical study on the effect of substitutional doping by N or B, the conductivity decreases less than 1 order for the concentration up to 4% with the localization length on a submicrometer order.[23] For the vacancy effect, the conductivity increases by more than 1 order with the concentration up to 0.5% due to enhancement of carrier density by midgap states, but it decreases and saturates to a certain value at higher concentration due to the major role of vacancy scattering.[24] Experimentally the temperature-dependent conductivity was explained by the variable range hopping model.[13] This model suggests that the transport occurs via consecutive tunneling between localized states. Since the experimental and theoretical results did not closely match, it is important to determine the transport behavior in RGO with more realistic structural models that have vacancies and residual O impurities as indicated by the experiment.[17]

With regard to the factors discussed above, we here investigate the electron transport of HT-RGO. No oxygen groups on the

basal plane except for the residual edge oxygen groups are assumed for the atomic structure. If we apply the known 10:1 C/O atomic ratio to a RGO flake of circular shape, its radius is 2.1 nm, where oxygen atoms are assumed only at the circumference and there is no vacancy defect. Since this size is too small, we need to allow vacancy defects where extra edge oxygen groups are introduced to passivate C dangling bonds. The edge oxygen group is assumed to be the ether form having the largest binding energy among various forms, as shown in the upper part of Figure 1 based on our recent study.[17] Under this model, the concentration of vacancy is estimated to be about 3% by taking into account the 10:1 C/O ratio. The vacancy defects and O impurities result in strong localization of electrons, while the vacancy is shown to be the main factor, as will be shown.

Two theoretical studies are carried out to study HT-RGO. One study is an ab initio calculation package (VASP)[25] based on DFT within the local density approximation (LDA),[26] which is used for detailed ground-state analysis of small periodic systems. The other study is the POSTRANS quantum transport calculation package[27,28] based on nonequilibrium Green's function (NEGF) formalism,[29−31] which has been used for electron and spin transport in large systems.[32,33] This approach is used to study the electron transport in the present large system with random defective sites with the nearest neighbor π orbital tight binding (π-TB) Hamiltonian as well as DFT. The tight binding scheme requires an accurate O−C hopping parameter that is obtained by a fitting procedure to reproduce ab initio band structures.

In the DFT study, vacancy alone creates σ and π dangling bond states at the Dirac point. Substitution of edge C atoms by O passivates σ dangling bonds and shifts down all electronic energy levels by 1.0 eV similar to the N doping effect (see Figure S1, Supporting Information). Also our previous DFT study of the edge-oxidized graphene nanoribbon shows that the O-p_z orbital has a significant hybridization with the C-π orbital.[34] Thus, we introduce two π-TB parameters to be fitted: the O−C hopping parameter (t_{OC}) and the onsite energy of O (ε_O). From the LDA energy eigen values of largely separated C and O atoms, the value of $\varepsilon_O = -4.0$ eV was extracted (the onsite energy of C is set to
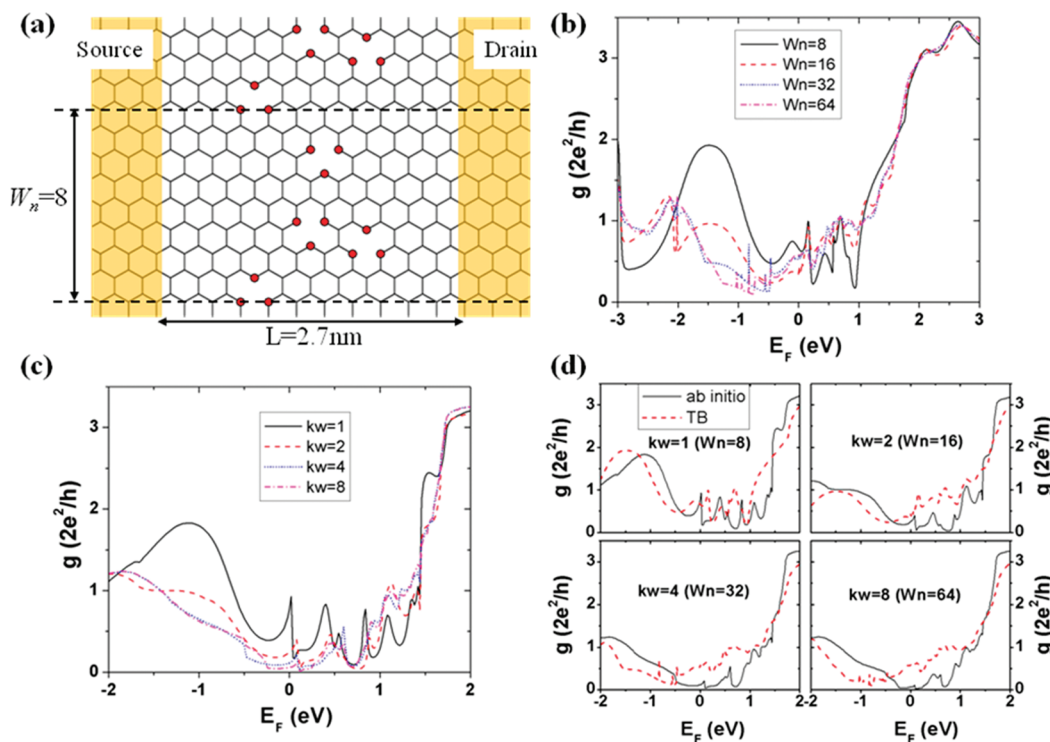
Figure 2. (a) Device structure used for transport simulation. Source and drain electrodes consist of semi-infinite ideal graphene sheets, and the scattering region of the reduced graphene oxide is disordered by defect type I as shown in Figure 1. For the purpose of a convergence test with the number of transverse eigenmodes, we choose a rather short channel ($L = 2.7$ nm) and periodic unit of eight zigzag chains ($W_n = 8$) along the width direction. (b) Normalized π-TB conductances with increasing the periodic width and sampling Γ point only for the transverse k-grid. The smallest periodic unit ($W_n = 8$) is duplicated by two, four, and eight times for larger periodicities of $W_n = 16$, 32, and 64, respectively. (c) Ab initio NEGF conductance with fixing the periodic width ($W_n = 8$) but increasing the transverse k-grid (k_w). (d) Comparison between ab initio and π-TB NEGF results for each periodic condition.

zero). The appropriate ratio of t_{OC}/ε_O is determined to obtain the consistent C-π band dispersion near the Fermi level between DFT and π-TB methods. For each of four model structures shown in Figure 1, where a 4×4 periodic supercell was used to obtain band structures, we find that the use of $t_{OC} = -2.2$ eV and $\varepsilon_O = -4.0$ eV gives a reasonable agreement, and their comparisons are shown in the lower part. The obtained π-TB bands lie 1.0 eV higher than the corresponding ab initio bands, and we shift down the π-TB energy eigenvalues by 1.0 eV. This approach is applied throughout this paper.

As for the transport simulation using the NEGF formalism, we obtain the retarded Green's function G by

$$G = \left[E - H - e\phi - \sum_S - \sum_D \right]^{-1}$$

where $\Sigma_{S(D)}$ are self-energies due to the interactions between the channel and source (drain) electrode. By varying the external gate potential ϕ or the Fermi level E_F, we compute the electrical conductance of the open system with

$$g(E_F) = \frac{2e^2}{h} \mathrm{tr}\{ G\Gamma_S G^\dagger \Gamma_D \}$$

where $\Gamma_{S(D)} = i[\Sigma_{S(D)} - \Sigma_{S(D)}^\dagger]$ are broadening matrices.
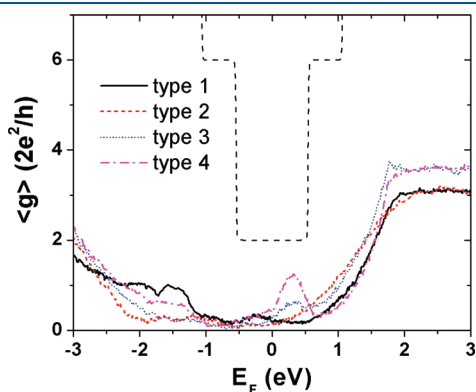
The device structure for our transport simulation is given in Figure 2a. Source and drain electrodes consist of semi-infinite ideal graphene sheets at both sides, and there is a scattering region in the middle with a specific length $L = 2.7$ nm in this case. In order to model the two-dimensional GO channel, the periodic

boundary condition is adopted along the transverse direction. Correspondingly, the convergence with respect to the number of transverse eigen modes needs to be checked. In our π-TB NEGF program the number of transverse eigen modes is controlled by varying the periodic width with the Γ point sampling. Thus, we first choose a rather small periodic width, eight zigzag chains ($W_n = 8$), as indicated in Figure 2a. Within this periodic width there are four arbitrary chosen defective sites of type I, which gives a C/O ratio of 12.6 inside the scattering region. Then we consider two, four, and eight duplicates of the eight zigzag chains as a new periodic width to introduce more transverse eigen modes, which are denoted as $W_n = 16$, 32, 64, respectively. The periodic width of $W_n = 8$, 16, 32, or 64 corresponds to an effective transverse k-grid (k_w) of 1, 2, 4, or 8, respectively, based on the smallest periodic width ($W_n = 8$). Their normalized conductances are shown in Figure 2b. We note that $W_n = 32$ (or $k_w = 4$) gives a well-converged shape, which corresponds to the periodic width of 6.7 nm. We have double-checked this conclusion with our ab initio transport program which allows finite k-point sampling. As shown in Figure 2c, the converged curve shape can be seen consistently at $k_w = 4$. From the comparison between π-TB and DFT NEGF results (Figure 2d), they qualitatively match well for each k-point sampling. Thus, our π-TB method is quite suitable.

On the basis of the π-TB NEGF method, the transport property of reduced graphene oxide is simulated for each defect type of Figure 1. The defects are introduced at random sites with sufficient intervacancy distance to avoid O—O bonds while
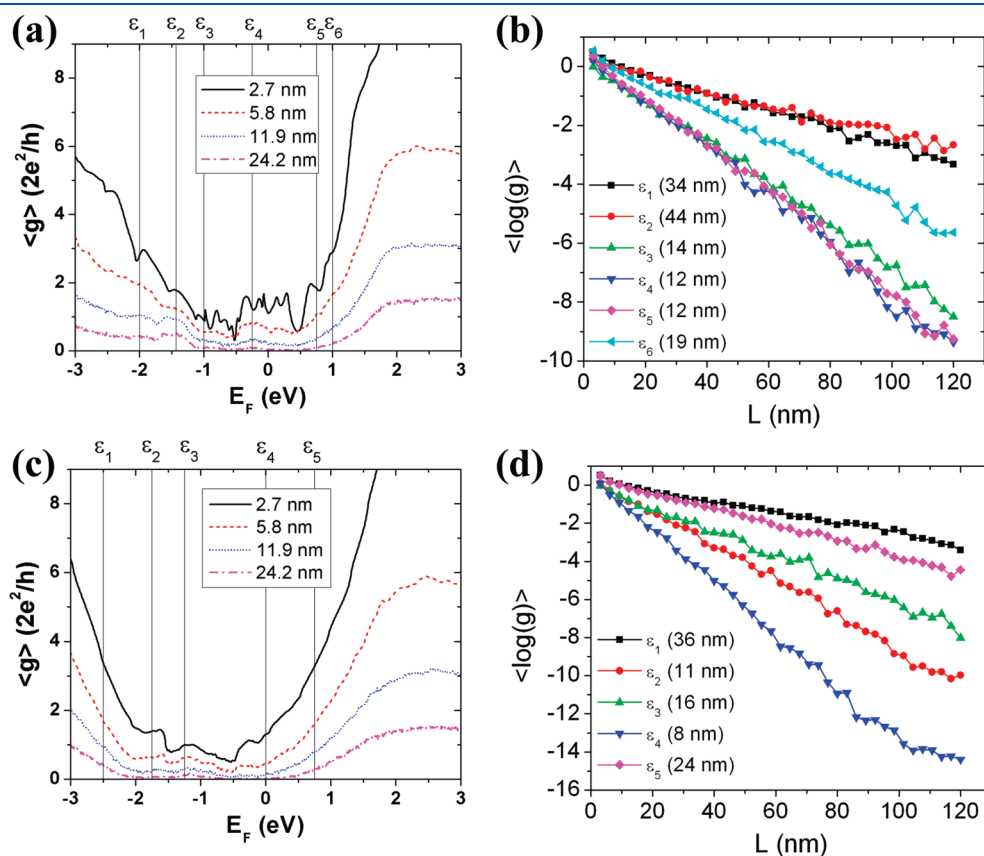
retaining the 10:1 C/O ratio. The periodic width of $W_n = 32$ is adopted. For a given channel length L, the average conductance $\langle g \rangle$ is obtained over 100 samples with different defect configurations. In Figure 3, the average conductances are shown for four defect types when the channel length is fixed as $L = 11.9$ nm. The overall shape is similar irrespective of the defect types, and the electron has a higher $\langle g \rangle$ than that of the hole. Its asymmetric

shape is attributed to a higher density of states (DOS) for the electron than for the hole, as can be seen in the band structures of Figure 1. It is caused by O substitution impurities, because the vacancy itself gives a symmetric shape. This effect of O is similar to the case of N substitution in graphene[23] and carbon nanotubes[35] (see Supporting Information). The O substitution itself introduces more electrons and increases the Fermi level above the Dirac point. However, additional neighboring vacancy defects such as in our system give rise to a smaller coordination number (i.e., 2). As a result, the unpaired nonbonding states of the O atom appear at the Fermi level, whose possible origin has been suggested to be the polarization effect caused by quantum entrapment.[36] We confirm that such states are localized as usual. Although minor conductance peaks near $E_F = 0$ eV can be seen in Figure 3 from those states, they vanish at longer channel length as described in the following paragraph. Behavior in which O-induced states are localized due to vacancy defects is similarly seen for all defect types. Assuming minor dependence on the defect type, we choose types I and II to analyze the conductance with varying channel length, which are metallic and semiconducting, respectively (shown in Figure 1), and the results are discussed below.

In Figure 4a and 4c, we show $\langle g \rangle$ with an increasing channel length from 2.7 to 24.2 nm. For a short channel length, no transport gap appears, but significant transport gap starts to appear at $L = 24.2$ nm. This indicates that localized states dominate in the gap region. Such localized states are spatially extended to a specific range, characterized by the localization length (L_c).

Figure 3. π-TB NEGF conductance averaged over 100 random configurations of reduced graphene oxide for the four different defect types shown in Figure 1. See Figure 2a for the schematic device structure in the case of defect type I. The periodic width and the channel length are fixed as $W_n = 32$ and $L = 11.9$ nm. The conductance of ideal graphene is shown by the black dashed line.

Figure 4. (a) Average conductance over 100 random samples ($\langle g \rangle$) of type I for four channel lengths $L = 2.7, 5.8, 11.9, 24.2$ nm. (b) Average of logarithmic conductance ($\langle \log(g) \rangle$) versus channel length for the Fermi levels indicated by the vertical lines in panel a. The same plots are given in panels c and d for type II.
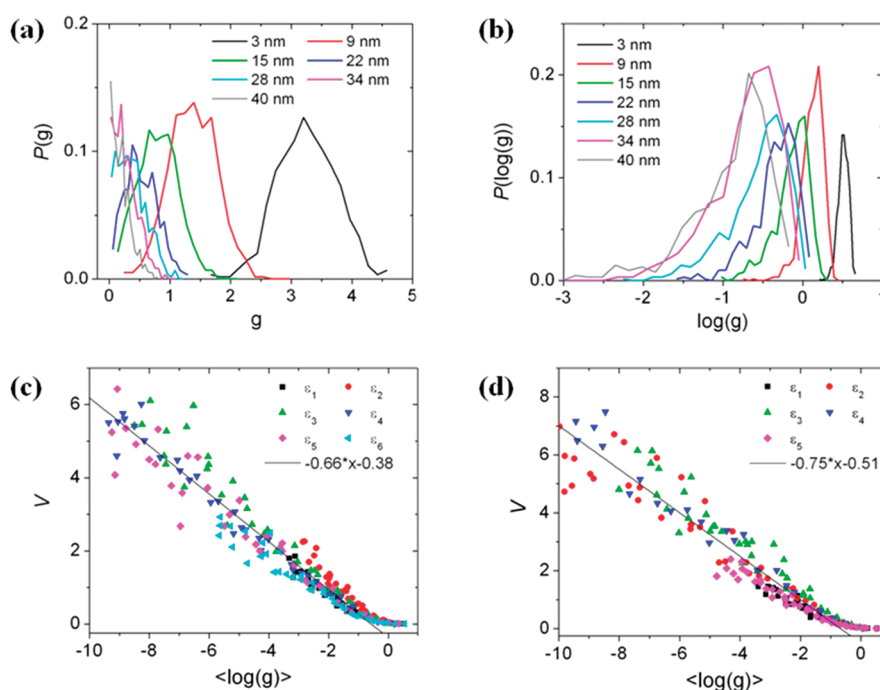
Figure 5. Probability distributions against (a) normal conductance $P(g)$, and (b) logarithmic conductance $P(\log(g))$. For each of the channel lengths varied from 3 to 40 nm, 600 random configurations of defect type I have been used and the conductance is computed at energy level ε_1 (see Figure 4a). (c) Variance $V = \langle \log^2 g \rangle - \langle \log g \rangle^2$ versus $\log(g)$ for defect type I; (d) the same plot for type II. One hundred random configurations for each channel length varied from 3 to 120 nm are generated to compute the conductance at the energy levels indicated in Figure 4a and 4c.

In our case, when the disorder strength is kept almost equal among different channel lengths, the transport behavior will be characterized by the channel length. For example, it belongs to the strongly localized regime for a channel length greater than L_c. With extensive variation of the channel length up to 120 nm, we plot $\langle \log(g) \rangle$ against L in Figure 4b and 4d for the specific energy levels indicated by the vertical dashed lines in Figure 4a and 4c, respectively, where the scaling law of $\langle \log(g) \rangle \sim -L/L_c$ is expected for the strongly localized regime. The exponentially decreasing conductance is verified, and the extracted localization length L_c ranges from 10 to 40 nm in our analysis. Interestingly, the conductance decays about 6 orders more for defect type II compared to type I, as in Figure 4b and 4d. This is likely to be the effect of the semiconducting band structure for the periodic model of type II as shown in Figure 1.

We note that such strong localization can be further confirmed by statistical analysis. For an ensemble of random configurations with equal disorder strength, the probability distribution of logarithmic conductance $(\log(g))$ rather than the conductance itself (g) should exhibit a Gaussian shape with a mean value of $\langle \log(g) \rangle$ in the case of the strongly localized regime.[37] In this respect, we choose defect type I and energy level ε_1 (see Figure 4a), and 600 random configurations are generated for each channel length where we vary the length from 3 to 40 nm. The obtained probability distributions about g and $\log(g)$ are shown in Figure 5a and 5b, respectively, for each length. Figure 5a shows that the distribution $P(g)$ exhibits a strong deviation from the Gaussian beyond a certain length, but it becomes close to a Gaussian shape when it is plotted against $\log(g)$, Figure 5b. This would be an indication of transition to the strongly localized transport and occurs at a length of about 20 nm. This is also comparable to the previously obtained localization length $L_c = 34$ nm in Figure 4b. Another indication of strong localization comes from the fact that $\langle \log(g) \rangle$

and its variance $(V = \langle \log^2 g \rangle - \langle \log g \rangle^2)$ have a relationship $V = A \langle \ln g \rangle^{\alpha} + B$ irrespective of the channel length, where the exponent α varies in the literature.[38] So we generate 100 random configurations of defect types I and II for each channel length varied from 3 to 120 nm to obtain V versus $\langle \log(g) \rangle$ data at the energy levels indicated in Figure 4a and 4c. The data gathered for the whole channel lengths are plotted in Figure 5c and 5d for types I and II, respectively. One can see approximately the linear scaling even though the ensemble size is as small as 100. Therefore, we suggest that all level states indicated in Figure 4a and 4c are strongly localized.

In transport experiments of reduced graphene oxides, the variable range hopping (VRH) was pointed out as a plausible charge transport mechanism from the temperature-dependent measurements.[13,39,40] Further experiments have shown that the single layer sample consists of disordered regions with intact graphene regions, which is consistent with detailed inspection of the atomic structure.[41,42] Thus, it was suggested that VRH occurs only in part of the sample and the resistivity is mainly caused by the disordered regions where the carrier hopping takes place via localized states. The size of the disordered regions was deduced to be about 10 to 20 nm.[41] Our model structures can be considered as the disordered regions, where the calculated localization length near the $E_F = 0$ eV is a little less than or comparable to the experimentally deduced size of the disordered regions. This means that the transport mechanism within the disordered regions is carrier hopping through localized states, and this will give rise to most of the resistance over a whole sample under the assumption of negligible resistance in intact regions. In other words, our obtained carrier localization length is consistent with experimentally observed transport behavior.[13,39,40] Although the real structure of defects is not known, such agreement allows the defects investigated in this work to be a probable candidate, as also proposed in a recent experiment.[17]
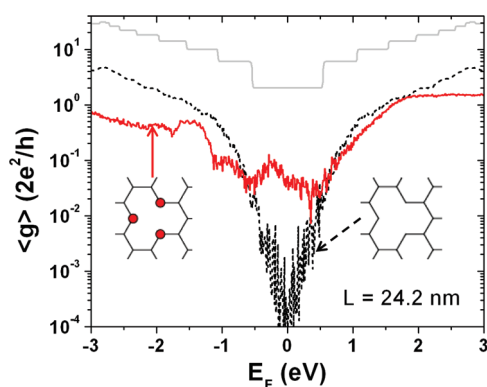
Figure 6. Average conductances of type I reduced graphene oxides with (red solid) and without (black dashed) oxygen substitution of edge carbon atoms, as represented in the inset, for a channel length of 24.2 nm. The gray line indicates the ballistic conductance of ideal graphene.

Finally, we investigate the relative importance of vacancy defects and oxygen impurities in causing the strong localization. For this purpose, we have performed a comparative model study of the type I defect by replacing the edge O atoms with C and retaining the vacancy defects, as shown in the inset of Figure 6. In Figure 6, we present two conductance curves with and without O substitution for $L = 24.2$ nm. The two curves have almost the same magnitude, though the hole conductance is a little larger in the case without O. From the result of almost the same order of magnitude in the two cases, the vacancy is shown to be the main factor inducing the localization and correspondingly degrading the conductivity. This finding is consistent with the report that it is difficult to reach the strong localization regime by increasing the B or N doping concentration,[23] while the conductivity is strongly suppressed with increasing vacancy concentration.[42] Also scanning tunneling spectroscopy has shown that vacancy defects give rise to well-localized π orbital dangling bond states.[43,44] The significant impact of such states has been discussed in detail regarding various phenomena such as localization, catalytic enhancement, magnetism, etc.[45]

In summary, we have performed electron transport simulation of RGO with the most probable atomic structure which involves C vacancies and the O substitution of edge C atoms. Our results show strongly localized electrons with a localization length of 10−40 nm, and this localization is mainly caused by vacancy defects rather than O impurities.

■ ASSOCIATED CONTENT

ⓢ Supporting Information. Ab initio density functional theory study on the effects of monovacancy and O impurities on the electronic density of states. This material is available free of charge via the Internet at http://pubs.acs.org.

■ AUTHOR INFORMATION

Corresponding Author
*E-mail: kjcho@utdallas.edu.

■ ACKNOWLEDGMENT

■ REFERENCES

(1) Novoselov, K. S.; Geim, A. K.; Morozov, S. V.; Jiang, D.; Zhang, Y.; Dubonos, S. V.; Grigorieva, I. V.; Firsov, A. A. *Science* **2004**, *306*, 666.

(2) Berger, C.; *Science* **2006**, *312*, 1191.

(3) Coraux, J.; N'Diaye, A. T.; Busse, C.; Michely, T. *Nano Lett.* **2008**, *8*, 565.

(4) Kim, K. S.; Zhao, Y.; Jang, H.; Lee, S. Y.; Kim, J. M.; Kim, K. S.; Ahn, J.-H.; Kim, P.; Choi, J.-Y.; Hong, B. H. *Nature* **2009**, *457*, 706.

(5) Bae, S.; Kim, H.; Lee, Y.; Xu, X.; Park, J.-S.; Zheng, Y.; Balakrishnan, J.; Lei, T.; Kim, H. R.; Song, Y. I.; Kim, Y.-J.; Kim, K. S.; Ozyilmaz, B.; Ahn, J.-H.; Hong, B. H.; Iijima, S. *Nature Nanotechnol.* **2010**, *5*, 574.

(6) Schniepp, H. C.; *J. Phys. Chem. B* **2006**, *110*, 8535.

(7) Park, S.; Ruoff, R. S. *Nat. Nanotechnol.* **2009**, *4*, 217.

(8) Stankovich, S.; *Nature* **2006**, *442*, 282.

(9) Si, Y.; Samulski, E. T. *Nano Lett.* **2008**, *8*, 1679.

(10) Tung, V. C.; Allen, M. J.; Yang, Y.; Kaner, R. B. *Nat. Nanotechnol.* **2009**, *4*, 25.

(11) Li, D.; Muller, M. B.; Gilje, S.; Kaner, R. B.; Wallace, G. G. *Nat. Nanotechnol.* **2008**, *3*, 101.

(12) Hernandez, Y.; *Nat. Nanotechnol.* **2008**, *3*, 563.

(13) Gomez-Navarro, C.; Weitz, R. T.; Bittner, A. M.; Scolari, M.; Mews, A.; Burghard, M.; Kern, K. *Nano Lett.* **2007**, *7*, 3499.

(14) Stankovich, S.; Dikin, D. A.; Piner, R. D.; Kohlhaas, K. A.; Kleinhammes, A.; Jia, Y.; Wu, Y. *Carbon* **2007**, *45*, 1558.

(15) Gilje, S.; Han, S.; Wang, M.; Wang, K. L.; Kaner, R. B. *Nano Lett.* **2007**, *7*, 3394.

(16) Gao, W.; Alemany, L. B.; Ci, Lijie; Ajayan, P. M. *Nature Chem.* **2009**, *5*, 1.

(17) Acik, M.; Lee, G.; Mattevi, C.; Chhowalla, M.; Cho, K.; Chabal, Y. J. *Nat. Mater.* **2010**, *9*, 840.

(18) Boukhvalov, D. W.; Katsnelson, M. I. *J. Am. Chem. Soc.* **2008**, *130*, 10697.

(19) Xu, S. C.; Irle, S.; Musaev, D. G.; Lin, M. C. *J. Phys. Chem. C* **2007**, *111*, 1355.

(20) Paci, J. T.; Belytschko, T.; Schatz, G. C. *J. Phys. Chem. C* **2007**, *111*, 18099.

(21) McAllister, M. J.; *Chem. Mater.* **2007**, *19*, 4396.

(22) Rutter, G. M.; Crain, J. N.; Guisinger, N. P.; Li, T.; First, P. N.; Stroscio, J. A. *Science* **2007**, *317*, 219.

(23) Lherbier, A.; Blase, X.; Niquet, Y.-M.; Triozon, F.; Roche, S. *Phys. Rev. Lett.* **2008**, *101*, 036808.

(24) Jafri, S. H. M.; *J. Phys. D* **2010**, *43*, 045404.

(25) Kresse, G.; Hafner, J. *Phys. Rev. B* **1993**, *47*, 558.

(26) Ceperley, D. M.; Alder, B. J. *Phys. Rev. Lett.* **1980**, *45*, 566.

(27) Kim, W. Y.; Kim, K. S. *J. Comput. Chem.* **2008**, *29*, 1073.

(28) Kim, W. Y.; Kim, K. S. *Acc. Chem. Res.* **2010**, *43*, 111.

(29) Svizhenko, A.; Anantram, M. P.; Govindan, T. R.; Biegel, B.; Venugopal, R. *J. Appl. Phys.* **2002**, *91*, 2343.

(30) Datta, S. *Electronic Transport in Mesoscopic Systems*; Cambridge University Press: Cambridge, UK, 1995.

(31) Datta, S. *Quantum Transport: Atom to Transistor*; Cambridge University Press: Cambridge, UK, 2005.

(32) Kim, W. Y.; Kim, K. S. *Nat. Nanotechnol.* **2008**, *3*, 408.

(33) Min, S. K.; Kim, W. Y.; Cho, Y; Kim, K. S. *Nat. Nanotechnol.* **2010**, *6*, 162.

(34) Lee, G.; Cho, K. *Phys. Rev. B* **2009**, *79*, 165440.

(35) Avriller, R.; Latil, S.; Triozon, F.; Blase, X.; Roche, S. *Phys. Rev. B* **2006**, *74*, 121406(R).

(36) Sun, C. Q.; Sun, Y.; Nie, Y. G.; Wang, Y.; Pan, J. S.; Ouyang, G.; Pan, L. K.; Sun, Z. *J. Phys. Chem. C* **2009**, *113*, 16464. Sun, C. Q.; Fu, S.-Y.; Nie, Y. G. *J. Phys. Chem. C* **2008**, *112*, 18927.

(37) Somoza, A. M.; Prior, J.; Ortuno, M.; Lerner, I. V. *Phys. Rev. B* **2009**, *80*, 212201.

(38) Chase, K. S.; MacKinnon, A. *J. Phys. C: Solid State Phys.* **1987**, *20*, 6189.

(39) Eda, G.; Mattevi, C.; Yamaguchi, H.; Kim, H.; Chhowalla, M. *J. Phys. Chem. C* **2009**, *113*, 15768.

(40) Kaiser, A. B.; Gomez-Navarro, C.; Sundaram, R. S.; Burghard, M.; Kern, K. *Nano Lett.* **2009**, *9*, 1787.

(41) Gomez-Navarro, C.; Meyer, J. C.; Sundaram, R. S.; Chuvilin, A.; Kurasch, S.; Burghard, M.; Kern, K.; Kaiser, U. *Nano Lett.* **2010**, *10*, 1144.

(42) Do, V. N.; Dollfus, P. *J. Appl. Phys.* **2009**, *106*, 023719.

(43) Ugeda, M. M.; Brihuega, I.; Guinea, F.; Gomez-Rodriguez, J. M. *Phys. Rev. Lett.* **2010**, *104*, 096804.

(44) Niimi, Y.; Matsui, T.; Kambara, H.; Tagami, K.; Tsukada, M.; Fukuyama, H. *Phys. Rev. B* **2006**, *73*, 085421.

(45) Sun, C. Q. *Nanoscale* **2010**, *2*, 1930.